BeBeC-2018-S09

INVESTIGATIONS ON BEAMFORMING IN THE WIND TUNNEL USING MULTIPLE MICROPHONE ARRAY MEASUREMENTS

Lukas Kleine Wächter[1], Jörg Ocker[2], Dirk Döbler[3], Christof Puhle[3] and Gert Herold[1]
[1]Technische Universität Berlin, Straße des 17. Juni 135, 10623 Berlin, Germany
[2]Dr. Ing. h.c. F. Porsche AG, 71287 Weissach, Germany
[3] GFaI e. V., Volmerstraße 3, 12489 Berlin, Germany

Abstract

Beamforming using microphone arrays has become a standard method for investigating aeroacoustic sound sources on vehicles. The quality of such measurements can be improved by increasing the number of microphones. However, the actual improvement is not in a fair proportion to effort and costs of this method. Another approach is the usage of multiple measurements under identical conditions, shifting the position of an array with a fixed microphone geometry. In this paper, the possibilities of multiple microphone array measurements for aeroacoustic applications will be outlined. For this, simulations were applied to test calculation procedures for combining the individual acoustic maps. The resulting maps were analyzed in terms of beam width and dynamic range to generate suitable conditions for actual measurements. Furthermore, an experimental setup was created in the wind tunnel of Porsche AG to verify the results under actual measurement conditions.

1 Introduction

Identifying sound sources is a necessary step for optimizing the acoustic properties of vehicles. For that purpose, microphone-array measurements in wind tunnels using beamforming-algorithms have become a common method. Beamforming-based investigations in aeroacoustics put high requirements on the microphone array system. Due to the interaction of the flow with the vehicle bodywork, many sources with diverse sound pressure levels occur on the scenery. However, since the beamformer is not an ideal spatial-filter, an interpretation of resulting acoustic maps is often aggravated due to incorrectly reconstructed outputs, appearing in the form of non-real “ghost sources” [5]. Hence, corrections applied afterwards using deconvolution approaches are a common procedure [13]. In order to minimize the errors during measurements, arrays with a large number of microphones and optimized distributions are used, allowing a denser spatial sampling of the sound field [1]. However, the improvements due to an

increase of the microphone number is limited considering the disproportional rise of costs and construction efforts of such systems.

An alternative strategy concerning an improved spatial sampling of the sound field is a virtual increase of the microphone number by applying multiple measurements [9, 10]. Here, the sound field is successively measured by a single microphone array shifted to various positions. Assuming that the sound field is stationary and the sound sources do not move, each map will contain a stationary part due to the immobile sound sources and a variable part due to the location-dependent array point spread function. By combing these maps on the basis of averaging, the level of ghost sources can be decreased whereas the actual source level is nearly unmodified [7, 8].

In this contribution, the possibilities of multiple microphone array measurements for aeroacoustic applications will be outlined. After sketching the theoretical bases of different averaging-methods in section 2, these methods are compared in section 3 within the scope of simulations in terms of dynamic range and beam width. Section 4 comprises the results of actual measurements in the aeroacoustic wind tunnel of Porsche AG [2]. The findings are finally summarized in section 5.

2 Theory

The research of the present paper follows the *Average Beamforming* method according to CASTELLINI and SASSAROLI [6]. The method is based on the output B_N for each focus point $\vec{x}$ at each frequency ω calculated equally for all microphone array positions $n \in [1,N]$, using the standard beamforming approach

$$B_n(\vec{x},\omega) = \vec{\gamma}^*(\vec{x},\omega)\,\mathbf{C}_n(\omega)\vec{\gamma}(\vec{x},\omega), \tag{1}$$

with the steering vector $\vec{\gamma}$, its conjugate transpose $\vec{\gamma}^*$ and the cross-spectral matrix $\mathbf{C}_n$ at array position n. From this a combined beamforming output B_{Avg} can be calculated, using simple arithmetic averaging

$$B_{\mathrm{Avg}}(\vec{x},\omega) = \frac{1}{N}\sum_{n=1}^{N} B_n(\vec{x},\omega). \tag{2}$$

In addition to CASTELLINI and SASSAROLI two further variations of this averaging approach were considered, changing the weighting of local minima of the acoustic maps. Firstly, the combination B_{Geom} according to the geometric mean:

$$B_{\mathrm{Geom}}(\vec{x},\omega) = \sqrt[n]{\prod_{n=1}^{N} B_n(\vec{x},\omega)}. \tag{3}$$

In the second variation according to EVANS, HARTMANN and DELFS [11], only the minimal value at focus point $\vec{x}$ of all calculated maps is considered for the combined map B_{Min}:

$$B_{\mathrm{Min}}(\vec{x},\omega) = \min\left(B_n(\vec{x},\omega)\right). \tag{4}$$

3 Simulations

At first, simulations under free-field conditions were applied to examine the calculation procedures mentioned in eq. (2)-(4). Therefor, a test setup was created to benchmark the resulting maps in terms of beam width and dynamic range.

3.1 Simulation setup

The simulations were based on a subarray-geometry of the microphone array installed in the wind tunnel of Porsche AG. Therefore, 48 out of 192 microphones were chosen to generate a simplified, round-shaped geometry with an aperture $D = 1.3\,\mathrm{m}$.

The maximum amount of measurements was limited to five, considering the effort of a practical execution. The measurement points were arranged regularly at the shifting interval s in horizontal and vertical direction. Figure 1 gives an overview of the simulation setup and the distribution of measurement points. The shifting-interval s was assigned to $D/2$ depending on the array aperture D.

On that basis, four variations for combining the resulting acoustic maps were selected, consisting of an increasing number N of measurements. The averaging-methods (2),(3) and (4) were adapted to these variations to combine an overall, averaged map. Additionally, a beamforming approach according to (1) was applied at the "standard" measurement point 1 for creating a basis of comparison. An overview over the variations and the corresponding notations is given in table 1. Table 2 summarizes the data acquisition and processing parameters.

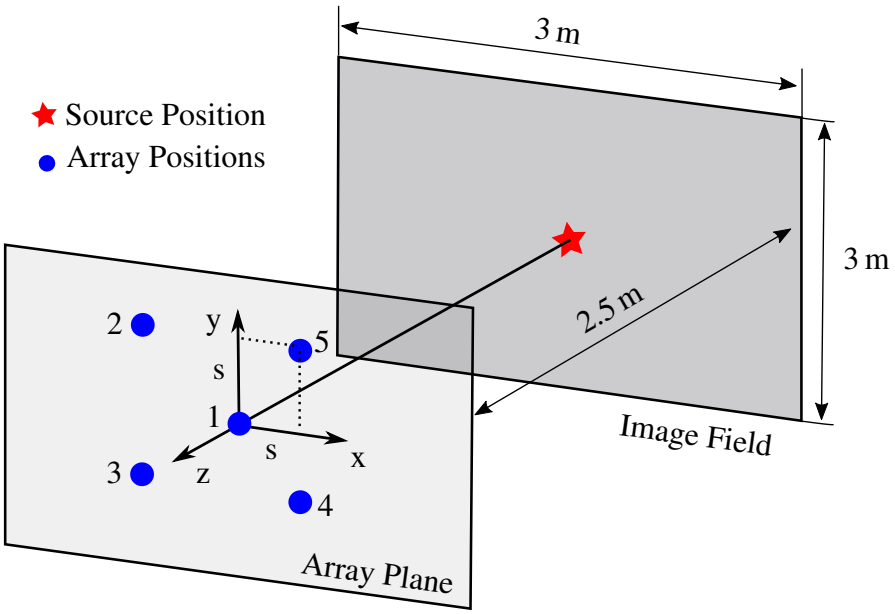

Figure 1: Overview of the simulation setup and array positions. Array positions depict the orientation of the array centre.

Table 1: Selected map-combinations based on the array position. The notation of measurement points matches fig. 1.

Combination	Averaged maps	Combination	Averaged maps
I	1,4	III	2-5
II	1,2,4	IV	1-5

Table 2: Data acquisition and processing parameters

Number of microphones	48	focus distance	2.5 m
Evaluated simulation time	5 s	Resolution of focus grid	0.01 m
Sampling rate	48 kHz	Source properties	white noise
FFT block size	2048 Samples		80 dB RMS
FFT window	von Hann	Algorithm	see (1)
	50% overlap		diagonal removal

3.2 Results

Dynamic range

In figure 2 the acoustic maps of Combination IV resulting from the different averaging methods are displayed exemplarily for four different third-octave bands, presented with a dynamic range of 25 dB. Corresponding maps calculated by standard beamforming without averaging are shown at the same dynamic range.

Without having a closer look at quantitative characteristics first, it can be seen that the application of multiple measurements connected with averaging leads to a reduction of side lobe levels for all methods and frequencies. However, there are clearly recognizable differences in the extent of reduction. Comparing the arithmetic averaging to the standard beamforming method, it is noticeable that in fact the side lobe level is decreased, but an elimination of side lobes can not be observed. In contrast to this, the remaining methods not only decrease the level of ghost sources but also "clean" the acoustic maps by eliminating side lobes, especially at higher frequencies. The minimum approach indicates the least amount of visible side lobes. The results lead to the conclusion that a high weighting of local minima in the average method is an effective strategy for improving the quality of acoustic maps.

This observation can be verified by evaluating the quantitative characteristics. Figure. 3 displays the dynamic range depending on the frequency for each method applied on combination IV. It can be seen that the arithmetic averaging leads to improvements of the dynamic range around 2-3 dB for all third-octave bands regarding standard beamforming. On the other hand, a significantly strong improvement of the dynamic range results from the minimum approach. The range increases to maximum amounts of 15 dB at 800 Hz and 12 dB at 5 kHz, the least increase can be recognized at a level of 5 dB for 2 kHz. The results of the geometric-averaging approach qualitatively match the curve of the minimum-method; however, its dynamic range is below the minimum between a range of 3 dB - 5 dB.

The fact that improvements of the geometric averaging and especially the minimum method

$f = 800\,Hz$

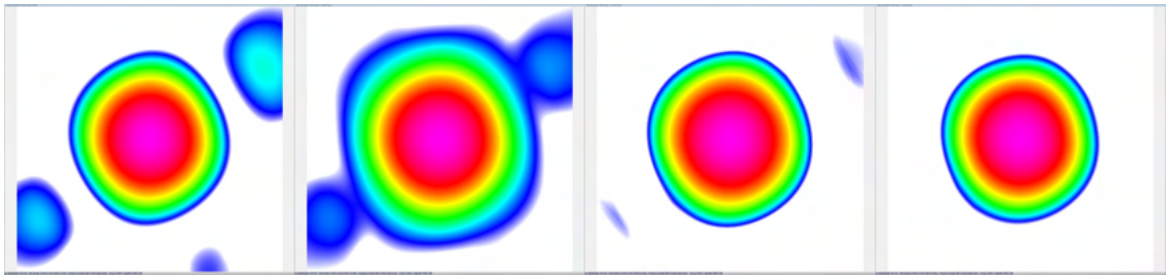

(a) Standard-Beamforming *(b)* Arithmetic *(c)* Geometric *(d)* Minimum

$f = 1600\,Hz$

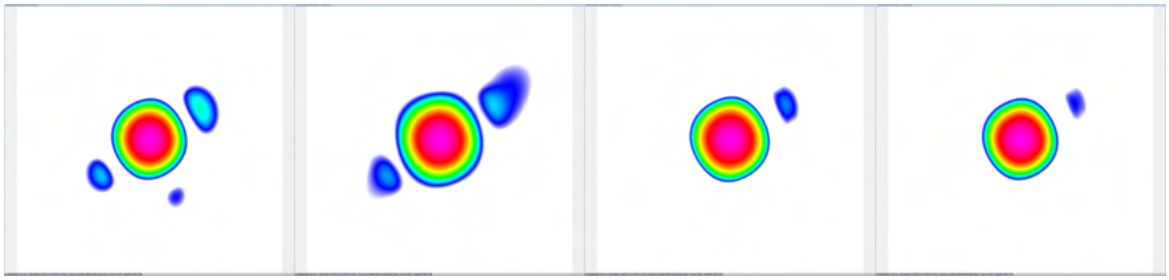

(e) Standard-Beamforming *(f)* Arithmetic *(g)* Geometric *(h)* Minimum

$f = 3150\,Hz$

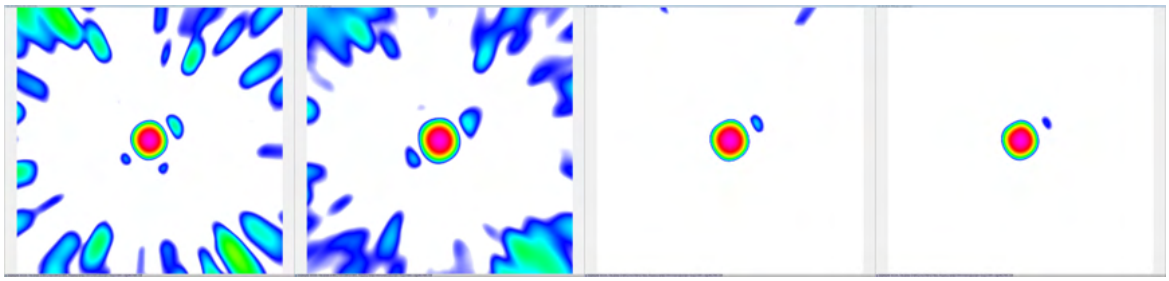

(i) Standard-Beamforming *(j)* Arithmetic *(k)* Geometric *(l)* Minimum

$f = 6300\,Hz$

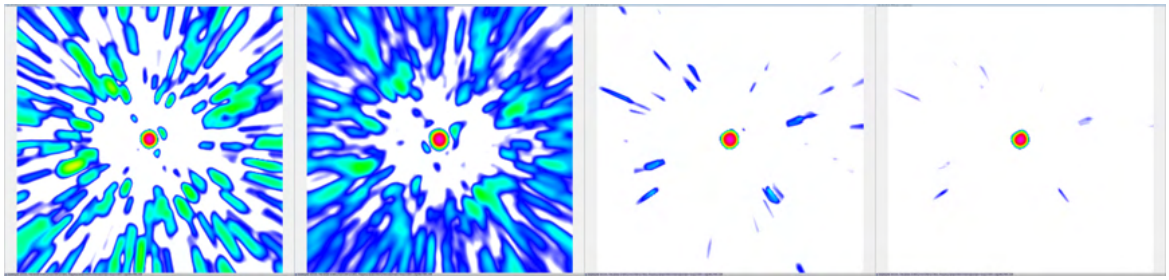

(m) Standard-Beamforming *(n)* Arithmetic *(o)* Geometric *(p)* Minimum

Figure 2: Comparison of the different averaging-methods. The figure shows the acoustic maps resulting from Combination IV according to Tab. 1. The dynamic range of all maps is 25 dB.

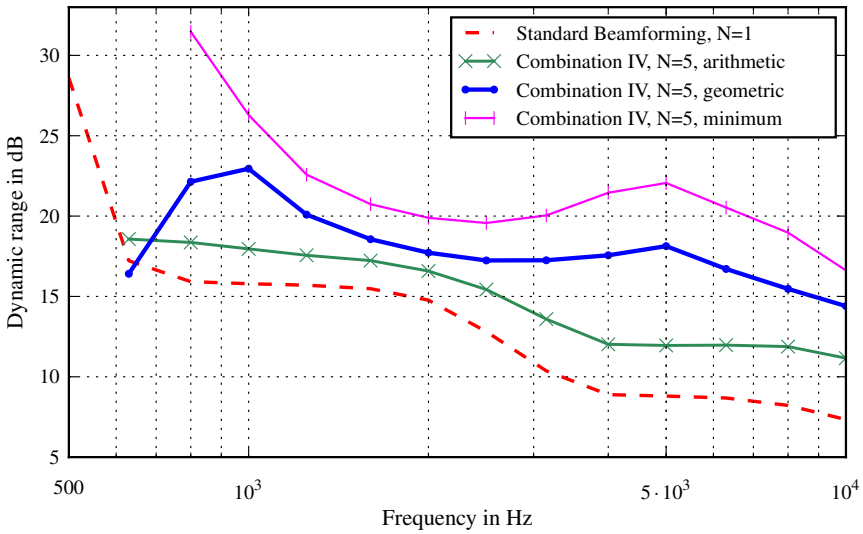

Figure 3: Dynamic range of combination IV based on different averaging methods. In addition, the dynamic range resulting from the standard-beamforming approach is displayed (red-dashed curve). Missing values at low frequencies result from a lack side of lobes in the image field.

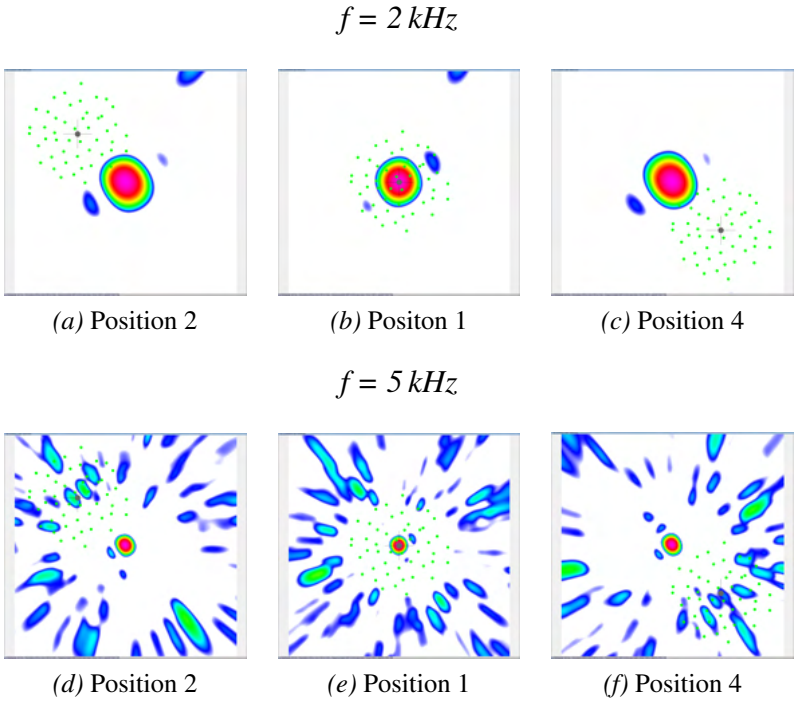

Figure 4: Single map beam patterns, depending on the array position. The figure exemplarily displays the findings of positions 1, 2 and 4 referring to table 1.

oscillate between a range up to 10 dB for different third-octave bands is due to the frequency- and location-dependent beam pattern of the single maps. Figure 4 displays the beam pattern resulting from standard-beamforming at array positions 1, 2 and 4 according to table 1. Additionally, the frequencies of 2 kHz and 5 kHz which mark points of mini-and maximum dynamic range increase are considered.

Comparing the maps at $f = 2\,\text{kHz}$, it can be seen that the beam patterns show optical similarities. For locations around the source, side lobes partially occur at a similar focus points, whereas the beam patterns at $f = 5\,\text{kHz}$ are more distinguishable, especially considering side lobes near the main lobe. It stands to reason that averaging of the acoustic maps at 2 kHz leads to less suppression of side lobes due to high signal outputs at identical focus points. On the other hand, at 5 kHz, more variable parts can be identified and consequently eliminated. Thus, for an effective side lobe suppression, it is desirable to generate as differing beam patterns as possible. For that purpose, an optimization of the array-position arrangement is a possible strategy that has to be considered for practical measurements.

A further attempt is an increase of the measurement points N in order to identify a higher amount of minimum signal outputs at a wide frequency range. Figure 5 illustrates the dynamic range for four different third-octave bands depending on the number of averaged measurements N according to table 1. Concentrating on the arithmetic approach, it becomes apparent that a higher number of averaged maps not necessarily leads to an improvement of the dynamic range. Especially at higher frequency bands the range does not improve despite a gain of information. Again, the minimum approach involves the most effective characteristics. Except for parts of the 3150 Hz band, the dynamic range nearly increases proportionally to the number of averaged maps, leading to a gain around 2 dB/N.

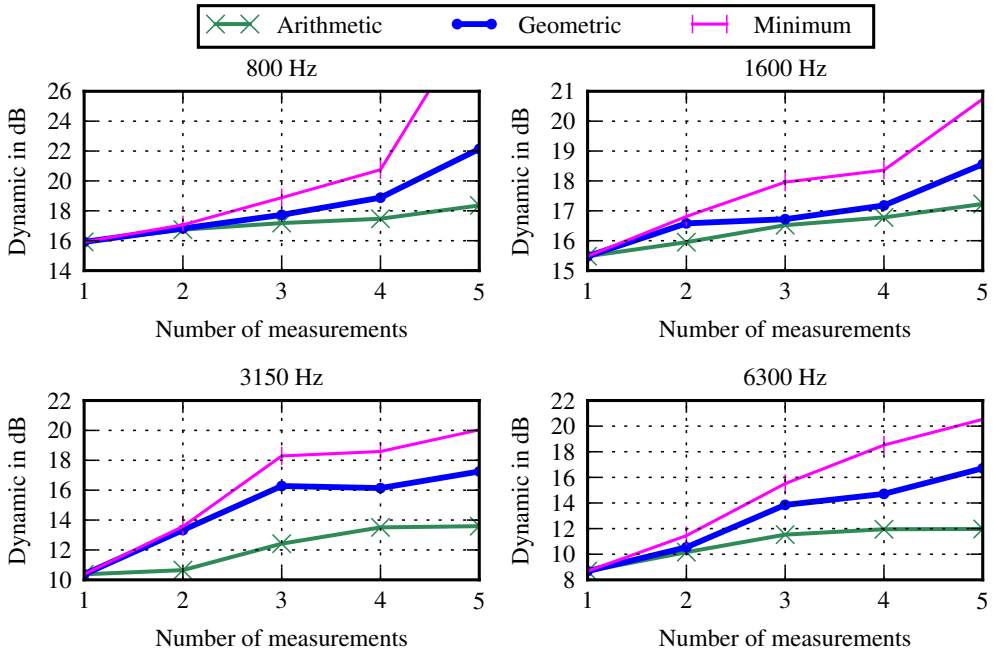

Figure 5: Dynamic range depending on the number of averaged maps.

Beam width

Beyond the dynamic range possible changes of the beam width due to averaging have to be considered. Figure 6 exemplarily displays the relative main lobe diameter variation of the combined maps for the combination IV with regard to the results of standard-beamforming. It can be realized that an enlargement of the beam width is a consequence of the combination-procedure. Especially at lower frequencies up to 2 kHz, the extension equals nearly 10 % for both arithmetic and geometric averaging method; the minimum approach leads to changes around 6 % for this frequency range. For the third-octave bands from 5 kHz to 8 kHz, no extensions can be seen for the minimum-curve, whereas the other methods both increase from a variation of 5 % to 12 %. As a consequence, the findings suggest that all averaging methods imply a slight decrease of the resolution capacity.

Focusing on the arithmetic and geometric approach, the results can be explained due to the position-dependent imaging-characteristics of microphone arrays. By analogy to optical imaging systems, the output depends on the viewing angle between source and system. The effect can be observed clearly in figure 4 at $f = 2000$ Hz. Without any shifting between source and array, the main lobe shows a circular structure, whereas a translation of the array leads to an elliptic deformation. When matching such acoustic maps based on arithmetic and geometric averaging, the non-overlapping parts are added to the map and consequently increase the beam width.

However, this solution does not explain the extension based on the minimum approach. By its definition, the output would only consist of the intersection of overlapping parts. A possible explanation attempt can be given considering sound pressure levels respective to the global maximum of the point-spread-functions.

Therefor, figure 7 illustrates the difference of the maximum sound pressure levels L_{Avg} of

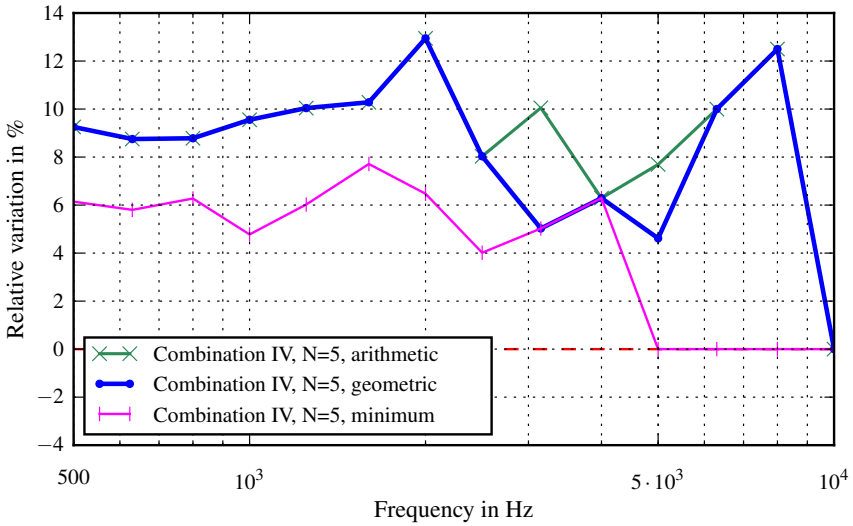

Figure 6: Relative Variation of main lobe diameter in horizontal direction. The figure displays the results of combination IV. In addition the level resulting from standard beamforming is shown (red-dashed line).

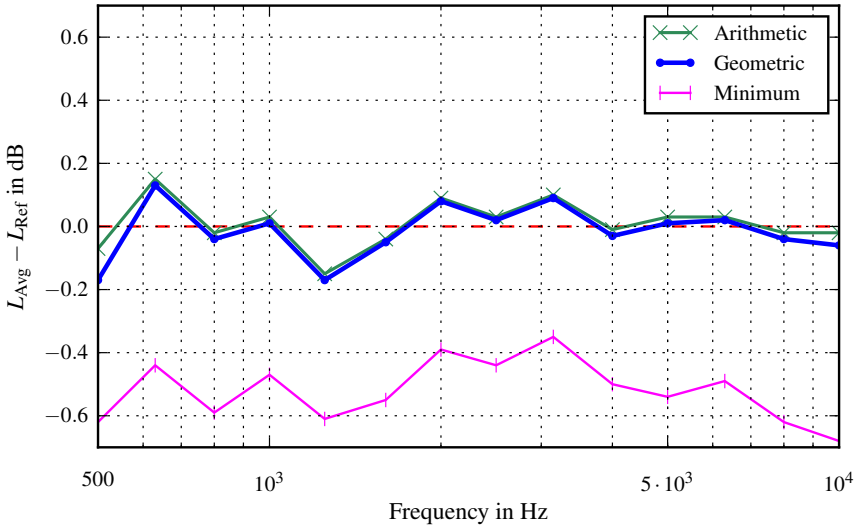

Figure 7: Differences of maximum sound pressure levels L_{Avg} of averaged maps regarding L_{Ref} (standard beamforming). The red-dashed line labels the standard beamforming level.

averaged maps regarding the equivalent levels L_{Ref} resulting from standard beamforming at position 1. While the arithmetic and geometric approach are qualitatively and quantitatively similar, showing insignificant changes of maximum levels around ± 0.2 dB, the minimum approach decreases the global maximum with an amount of 0.5 dB on average. Due to the fact that the beam width is measured at -3 dB beneath the global maximum, the findings discussed in figure 6 consequently result from slightly different reference levels. Hence, an enlargement of the beam width is a consequence despite the characteristics of the minimum approach. This explanation does not hold true for frequencies starting at 5 kHz. Thus, further investigations considering this effect are necessary.

4 Measurements at the Porsche Wind Tunnel

4.1 Measurement setup

Based on the findings discussed in section 3, measurements were performed at the aeroacoustic wind tunnel at Porsche Research Center in Weissach [2]. The microphone array system installed at the test section consists of three identical microphone arrays of dimension 5 m x 3 m, each equipped with 192 electret microphones and an integrated Full-HD camera. For the present research, one of those arrays was used to measure a scenery at various positions. The configuration used for that purpose is shown schematically in figure 8.

In reference to practically relevant setups, a SAE-based model was used to emulate the aeroacoustic characteristics of vehicles [3]. The model was so constituted that the acoustic characteristics of the side window could be investigated under the impact of wind stream. Hence, no exterior mirrors were mounted. Furthermore, a loud speaker was fixed out-of-flow at the window frame to generate a reproducible sound source at a known position. In order to quantify the array movement for the required microphone coordinate correction, a 3D laser scanner was

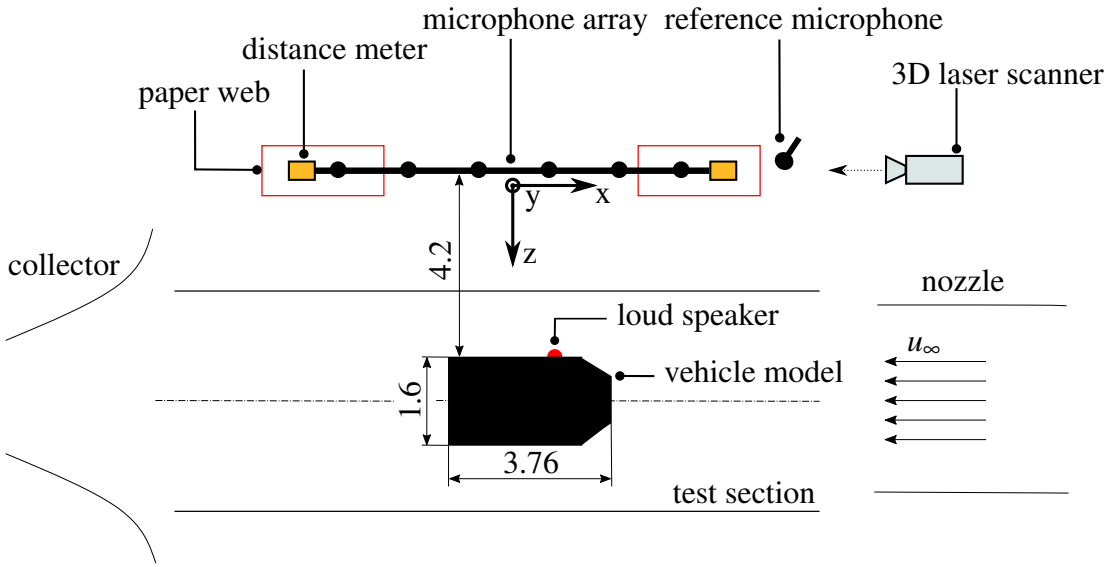

Figure 8: Schematic of the measurement setup (not true to scale, all values in m). The setup is presented from the topview.

used to measure the translations. For supervisory purposes the array movement was additionally measured with two distance meters and two paper webs to mark the respective measurement position. Moreover, an additional reference microphone was placed next to the array and not moved during the measurements.

Altogether, the scenery was measured at flow speeds of $u_\infty = 100\,\mathrm{km/h}$ and $u_\infty = 140\,\mathrm{km/h}$ at 10 different positions, including both vertical and horizontal translations of the array. The choice of positions was based on further simulations including the total amount of microphones [12]. In figure 9 an overview of the selected measurement point distribution and the translations regarding the "standard" position No. 1 is given.

4.2 Calculation

Table 3 summarizes the data acquisition and processing parameters. For each position a shear layer correction was executed before applying the averaging approach. Based on the promising results presented in section 3, the minimum method was utilized.

Table 3: Data acquisition and processing parameters for the measurement

Number of microphones	192	focus distance	4.2 m
Evaluated measurement time	10 s	Resolution of focus grid	0.01 m
Sampling rate	48 kHz	shear layer distance	1.5 m
FFT block size	2048 Samples	widening angle	9 °
FFT window	von Hann	algorithm	see (1)
	50% overlap		diagonal removal

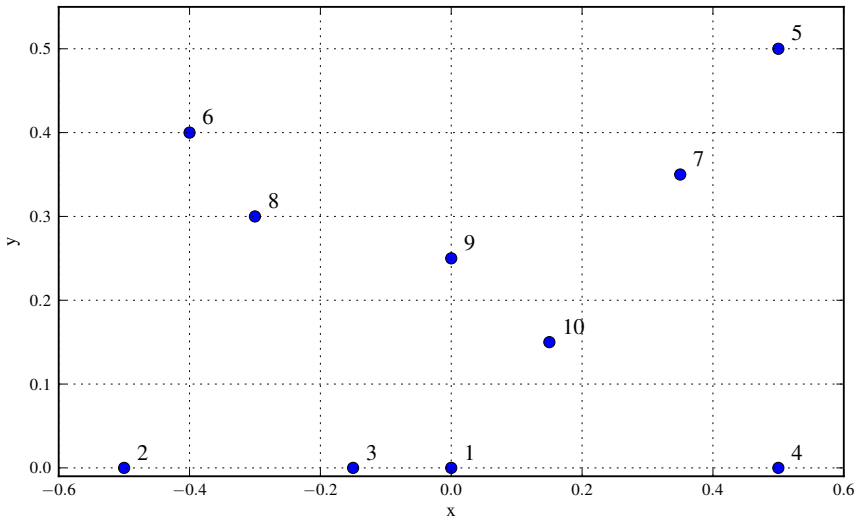

Figure 9: Overview on the measurement point distribution and its notation. The x-y-directions are corresponding to the orientation defined in figure 8 (all values in m).

4.3 Results at wind speed $u_\infty = 100\,{}^{km}/_{h}$

Figure 10 displays the acoustic map resulting from standard-beamforming applied on position 1 according to figure 9 at $f = 2500\,\text{Hz}$. As it turns out, five sources can be identified and associated clearly with components of the body work. Besides the loud speaker, sound is also emitted due to the impact of flow on the window frame and the pedestal of the model.

According to the findings of the minimum approach shown in figure 5, at first glance all measurements were averaged to an overall map to classify the results when the maximum of information is utilized. Figure 11 shows the corresponding acoustic maps in comparison to standard beamforming applied on position 1 at different frequencies.

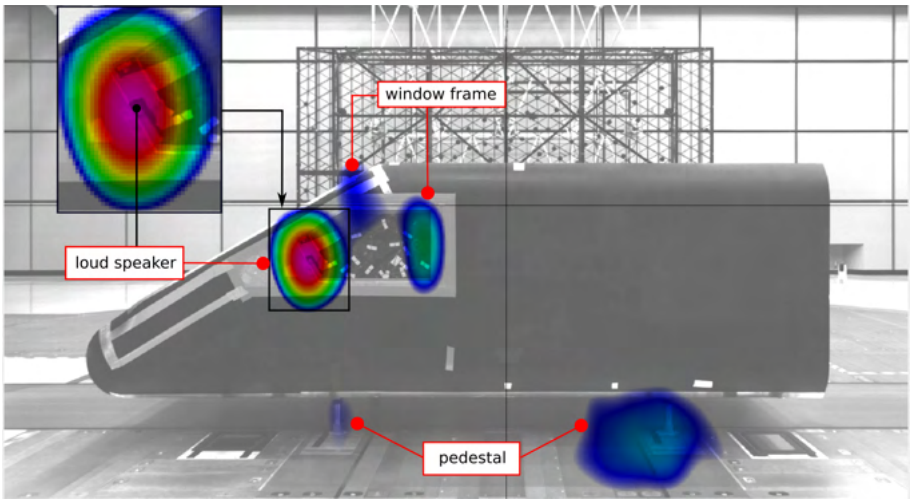

Figure 10: Overview of the detected sources. (2500 Hz, 17 dB)

f = 1250 Hz

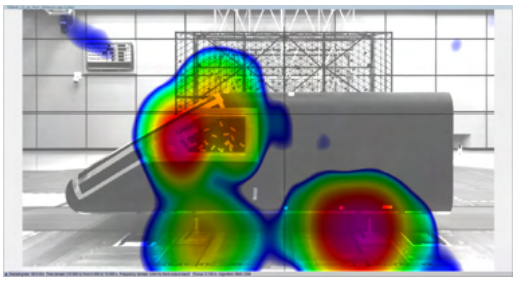

(a) Standard-Beamforming, N = 1

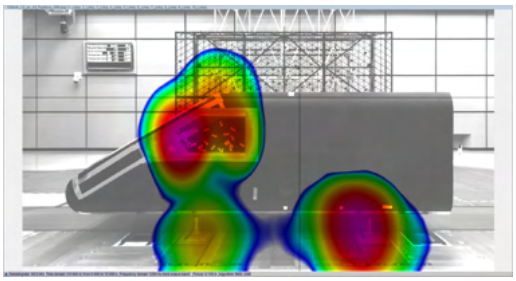

(b) Minimim-approach, N = 10

f = 2000 Hz

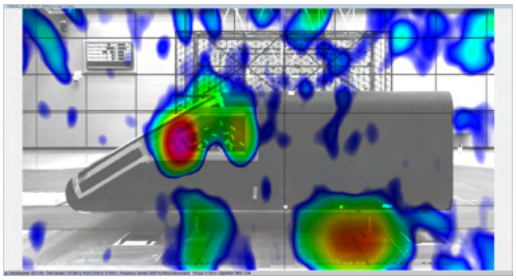

(c) Standard-Beamforming, N = 1

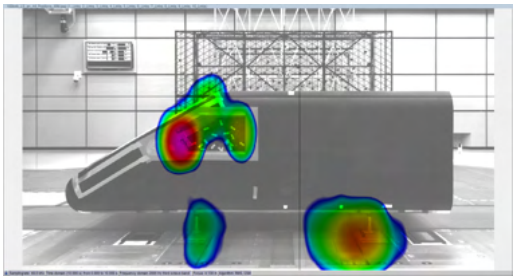

(d) Minimim-approach, N = 10

f = 4000 Hz

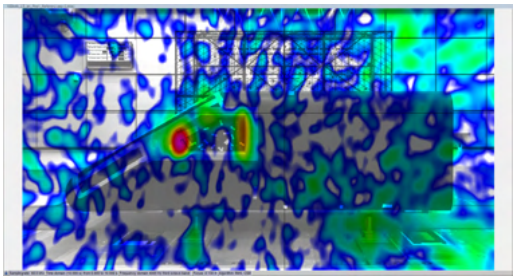

(e) Standard-Beamforming, N = 1

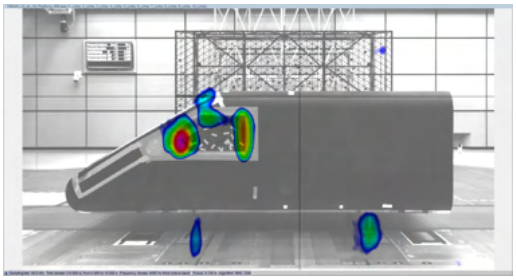

(f) Minimim-approach, N = 10

f = 6300 Hz

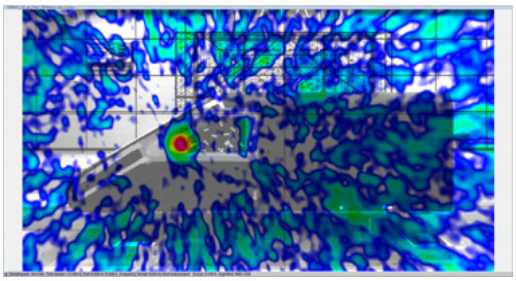

(g) Standard-Beamforming, N = 1

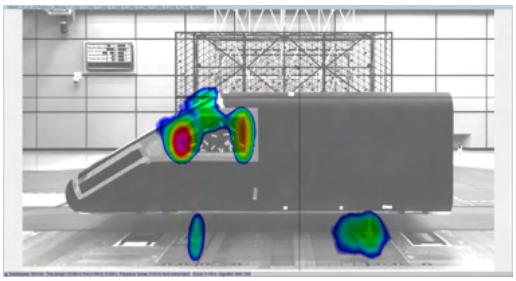

(h) Minimim-approach, N = 10

Figure 11: Acoustic Maps resulting from standard beamforming (left) and averaging of 10 measurements applying the minimum approach (right). The dynamic range of each map is 30 dB.

From a qualitative point of view, the results confirm the conclusions drawn on the basis of simulation. The method unmistakably leads to a significant improvement of acoustic maps because side lobes are suppressed and even eliminated. The effect essentially manifests at higher frequency bands, i. e. at $f = 6300\,\text{Hz}$. Here, the non-averaged map contains a high density of side lobes masking the majority of sources identified in figure 10. On the contrary, the corresponding averaged map is nearly entirely "cleaned" from side lobes; the sources can be observed completely at a high dynamic range without applying a deconvolution approach. At $f = 1250\,\text{Hz}$ and lower third-octave bands, the spreading and overlapping of sources is too pronounced so that the improvements can not be noticed as clearly. Even though side lobes are eliminated (see $f = 1250\,\text{Hz}$), nevertheless the averaged maps can not be interpreted unmistakably without deconvolution. The results also have to be rated considering cost and efforts of multiple measurements. In practice, 10 measurements would not be realizable despite the obvious benefits.

For that reason, two further combinations including less measurements are shown in figure 13 compared to the discussed ones. Firstly, the maps resulting from the average of positions $\{1,2,5,6\}$ are displayed to see the outcomes when the amount of information is more than halved. Secondly, the combination $\{1,2,4\}$ is presented because it only consists of horizontally shifted points, which can be arranged very easily during measurements. Figure 12 illustrates an adapted dynamic range for all combinations, starting at 2 kHz, to quantify the outcomes. Because the actual dynamic range is not defined for maps including multiple sources, the displayed values base upon figure 10, assuming that other outputs than the five verified ones appear due to side lobes. As a consequence, the results are only reliable regarding this reference, but not in absolute manners.

According to the observation in section 3, the results are well scalable. The average of all measurements leads to a maximum improvement, doubling the dynamic range at 2 kHz - 3.15 kHz. As expected, the most efficient combination regarding measurement lead times is the less efficient considering the improvements. The difference compared to standard beamforming

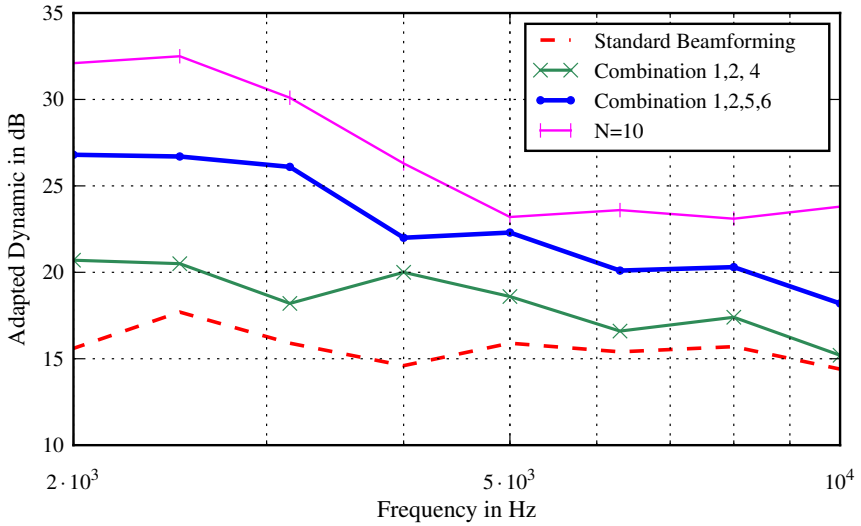

Figure 12: Adapted dynamic range for the third-octave bands from 2 kHz to 10 kHz .

$f = 3150\,Hz$

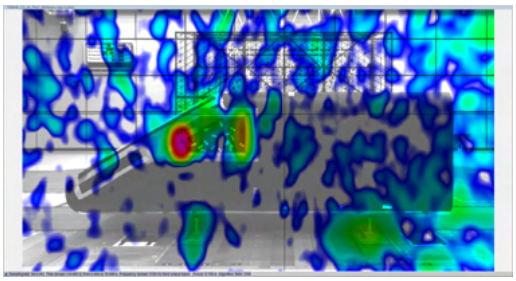

(a) Standard-Beamforming, N = 1

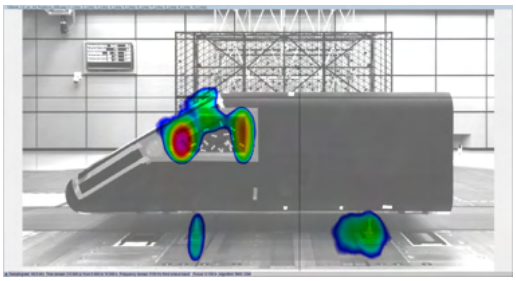

(b) N = 10

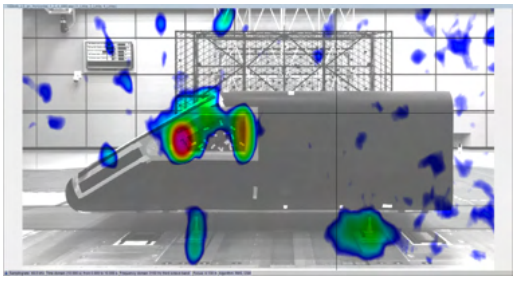

(c) Combination 1,2 and 4

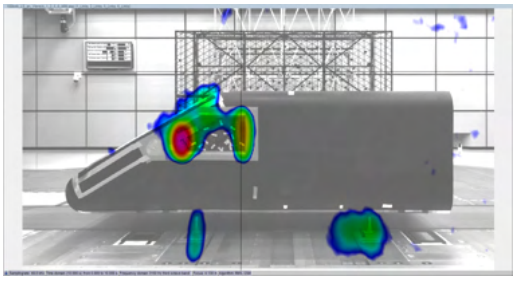

(d) Combination 1,2,5 and 6

$f = 6300\,Hz$

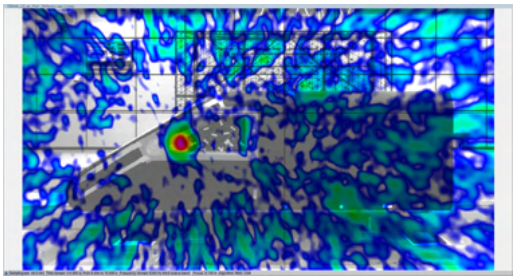

(e) Standard-Beamforming, N = 1

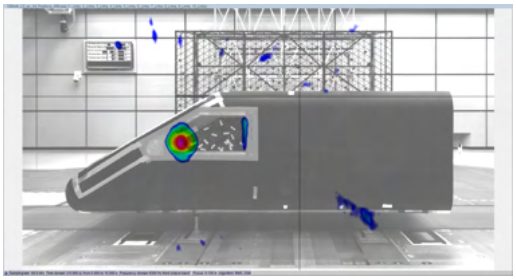

(f) N = 10

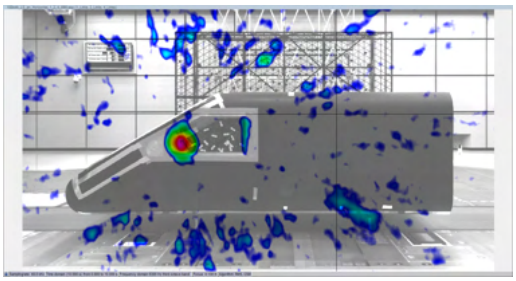

(g) Combination 1,2 and 4

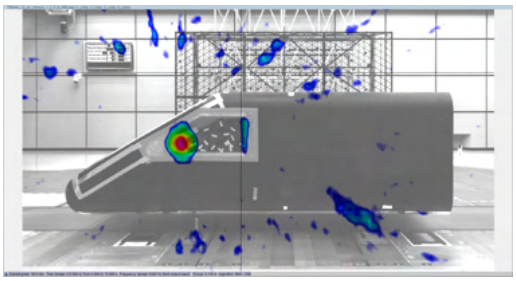

(h) Combination 1,2,5 and 6

Figure 13: Comparison of different combinations to standard beamforming at $u_\infty = 100\ ^{km}/_{h}$. The dynamic range of each map is 30 dB.

oscillates between values of 2 dB and 5 dB over the displayed frequency range, being near the reference level for frequencies starting at 6300 Hz. Despite this slight improvement, high side lobe levels only occur at discrete locations. The corresponding acoustic map at $f = 6300$ Hz (see figure 13) is visibly cleaned, being preferable to the standard method due to displaying previously masked sources at the window frame. Combination $\{1,2,5,6\}$ is a compromise between dynamic range improvements and an increased time requirement. The dynamic range improvement compared to the previous combination is nearly doubled, with a minimum increase of 5 dB. This observation leads to the conclusion that applying both horizontal and vertical translations of the array during measurements is an effective strategy, especially when the actual number of measurements is limited. This interpretation is supported considering the qualitative characteristics of the acoustic maps. Comparing figure 13 (b), (d) resp. (f), (h), it turns out that the reduced combination contains slightly more side lobes at the boundary of the image field. Beyond this, the reduced combination is nearly as "clean" as the combination leading to maximum dynamic ranges. As a further consequence, the efficiency of the measurement procedure can be increased on the basis of an optimized combination containing a practically realizable amount of array positions with an optimized distribution.

4.4 Results at wind speed $u_\infty = 140\ ^{km}/_{h}$

The combinations discussed in section 4.3 were further evaluated under the impact of flow speeds at $u_\infty = 140\ ^{km}/_{h}$ to investigate the applicability of the method under aggravated conditions. Figure 15 again illustrates the acoustic maps at the frequency bands shown before. Analogous to section 4.3, an adapted dynamic range was calculated based on verified sources for frequencies starting at 2 kHz. The findings are presented in figure 14.

Focusing on the qualitative properties of the maps at first, it turns out that the averaging method does not lose its efficacy over the increase of flow speed. Again the maps show an obvious reduction of side lobes, nearly entirely cleaned for the merge of 10 measurements.

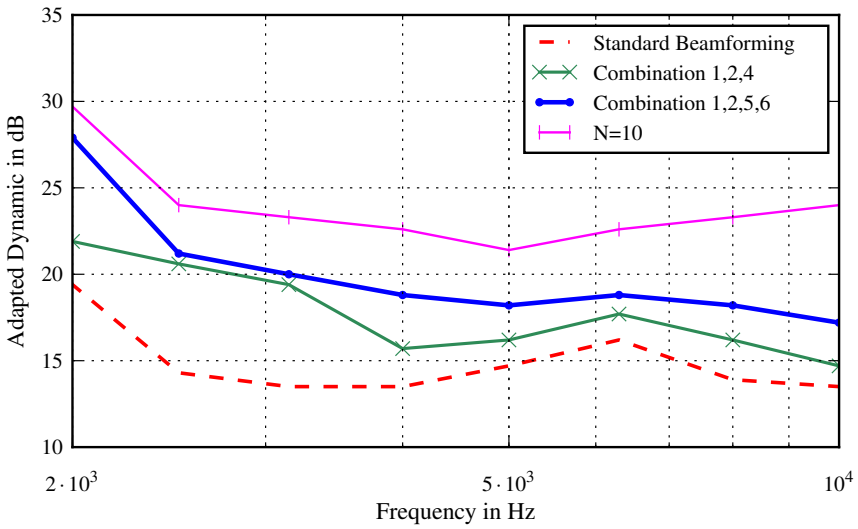

Figure 14: Adapted dynamic range for the third-octave bands from 2 kHz to 10 kHz .

Corresponding to the findings at $u_\infty = 100\ ^{km}/_{h}$, the combination $\{1,2,5,6\}$ including both horizontal and vertical translations is an efficient compromise between improvement and effort, showing slightly more side lobes than the average of all maps. The most time-saving setup $\{1,2,4\}$ leads to more distinct side lobes, but nevertheless is considerably improving the map compared to standard beamforming.

Considering the adapted dynamic in figure 14, it is notable that the curves match the trends discussed in figure 12 qualitatively. The improvement for combination N=10 oscillates between a range of 7 dB-10 dB, whereas combination $\{1,2,5,6\}$ involves a range between 4 dB - 8 dB depending on the frequency. The least effective method regarding this scale again is combination $\{1,2,4\}$ with improvements between 2 dB - 6 dB. As expected, the increase of flow speed does affect the possibilities of the averaging method. Comparing the maps shown in figure 13 and 15, it becomes apparent that the maps calculated at $u_\infty = 140\ ^{km}/_{h}$ contain more pronounced side lobes. Nevertheless, the method is also capable of improving the quality of acoustic maps at high, practice-oriented wind speeds, allowing an interpretation for high frequencies at high contrasts without applying a deconvolution approach.

5 Conclusion

In the present paper, the possibilities of multiple microphone array measurements for aeroacoustic applications were investigated. The method is an auspicious attempt for the improvement of beamforming-based investigations in wind tunnels. Within the scope of simulations under free-field conditions, it was shown that averaging of acoustic maps on the basis of a minimum approach, which only considers minimum signal outputs for the resulting map, is an effective strategy to suppress and even eliminate side lobes over a wide frequency range. In order to achieve high dynamic ranges, it is necessary to generate various beam patterns which can be obtained by either applying as many measurements at various positions as possible or selecting an accurate distribution of limited measurement positions, including both horizontal and vertical translations of the microphone array. As expected, the averaging approach is not capable of improving the optical resolution, the beam width is slightly expanded.

Furthermore, the procedure's efficiency was proven under actual conditions in the wind tunnel at different flow speeds. Averaged maps were nearly entirely cleaned from side lobes at dynamic ranges of 30 dB without the use of deconvolution, allowing the observation of previously masked sources. It is possible to obtain relative dynamic range improvements up to 12 dB, even when a realizable amount of four measurements is considered. However, the optical improvements due to side lobe elimination are restricted to higher frequency bands, approximately beginning at 2 kHz. Because the spreading of sources can not be minimized with basic averaging, interpretability of corresponding maps at lower frequencies suffers from the overlap of sources. Thus, a deconvolution approach still is necessary.

In this context the *Enhanced Beamforming* method according to [6] and [8] is an origin for further investigations. The approach is based on the combination of cross-spectral matrices before the actual beamforming and is a promising strategy for combining the benefits of multiple measurements and deconvolution algorithms.

f = 3150 Hz

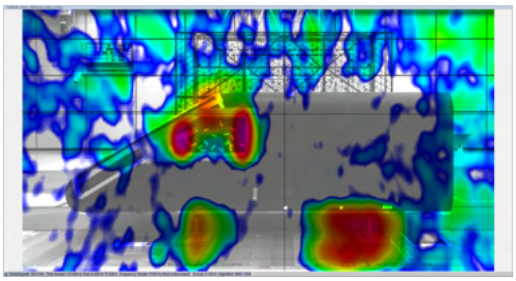

(a) Standard-Beamforming, N = 1

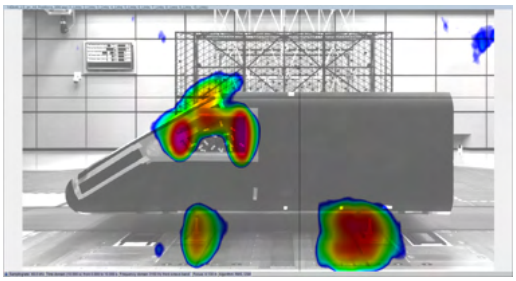

(b) N = 10

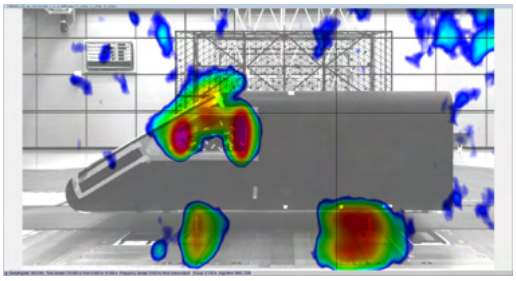

(c) Combination 1,2 and 4

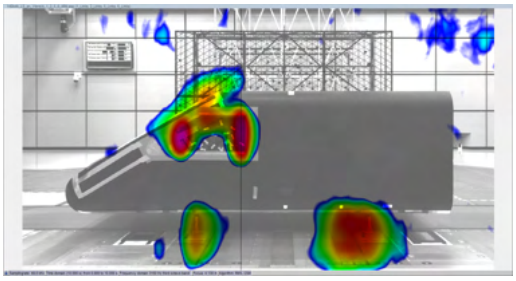

(d) Combination 1,2,5 and 6

f = 6300 Hz

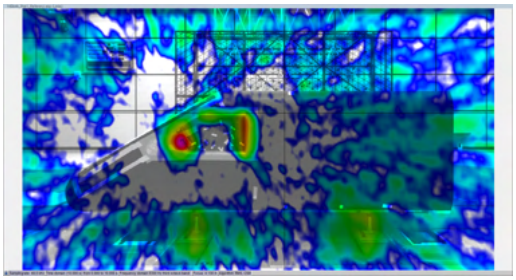

(e) Standard-Beamforming, N = 1

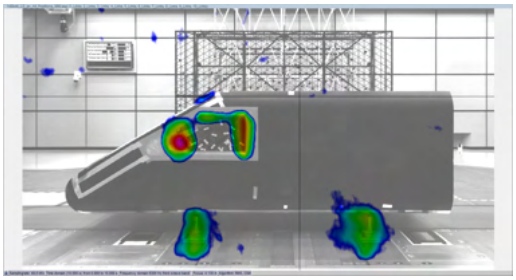

(f) N = 10

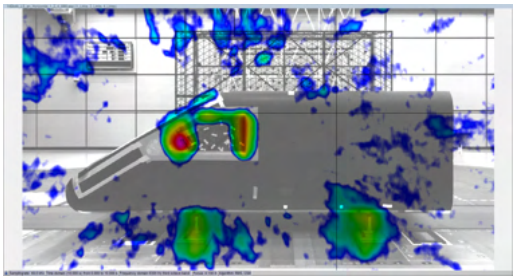

(g) Combination 1,2 and 4

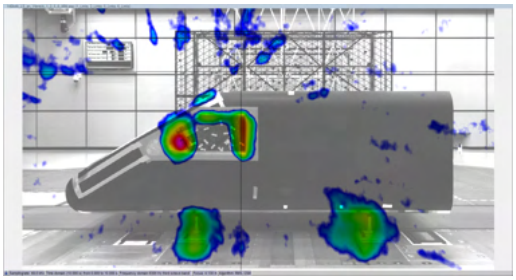

(h) Combination 1,2,5 and 6

Figure 15: Comparison of different combinations to standard beamforming at $u_\infty = 140\ ^{km}/_{h}$. The dynamic range of each map is 30 dB.

References

[1] J. OCKER, S. TILGNER: *The Porsche Wind Tunnel Microphone Array System.* Conference Paper Aachen Acoustics Colloquium (AAC) 2015, S. 135-151.

[2] H. STUMPF, P. RÖSER, T. WIEGAND: (2015): *The new aerodynamic and aeroacoustic wind tunnel of the Porsche AG.* 15. Internationales Stuttgarter Symposium. Proceedings. Springer Vieweg, Wiesbaden.

[3] M. HARTMANN, J. OCKER ET AL.: *Investigations of Sunroof Buffeting in an Idealised Generic Vehicle Model — Part I: Experimental Results*. Conference Paper of 29th AIAA Aeroacoustics Conference, May 5-7 2008, Vancouver B.C.

[4] A. LAUTERBACH, K. EHRENFRIED, K. KOOP: *Array Measurements in Wind Tunnels with Open Test Sections*.
Conference Paper of 2nd Berlin Beamforming Conference 2008, Berlin.

[5] E. SARRADJ: *A Generic Approach to Synthesize Optimal Array Microphone Arrangements*. 6th Berlin Beamforming Conference 2016, Berlin.

[6] P. CASTELLINI, A. SASSAROLI: *Acoustic source localization in a reverberant environment by average beamforming*.
Mechanical Systems and Signal Processing No. 24 (2010), Article ID 796-808.

[7] P. CASTELLINI, A. SASSAROLI, A. PAONESSA, A. PEIFFER, A. ROEDER: *Average beamforming in reverberant fields: Application on helicopter and airplane cockpits.* Mechanical Systems and Signal Processing No. 74 (2013), Article ID 198–210.

[8] J. KOKAVECZ, C. SPEHR: *Microphone Array Technology for Enhanced Sound Source Localisation in Cabins*. Conference Paper AIA-DAGA 2013, Merano.

[9] A. CIGADA, M. LURATI, F. RIPAMONTI, M. VANALI: *Beamforming Method: Suppression of Spatial Aliasing Using Moving Arrays.* Conference Paper of 2nd Berlin Beamforming Conference 2008, Berlin.

[10] D. DÖBLER, A. MEYER, G. HEILMANN, P. HÖHNA: *Dynamic beamforming using moving phased array with integrated 3D scanner.* Conference Paper of Aachen Acoustics Colloquium 2017, Aachen.

[11] D. EVANS, M. HARTMANN, J. DELFS: *Beamforming for point force surface sources in numerical data*. 2018, Manuscript in preparation.

[12] L. KLEINE WÄCHTER: *Untersuchungen zur Charakterisierung aeroakustischer Schallquellen durch Kombination von Mikrofonarraymessungen.*
Bachelor Thesis in collaboration with TU Berlin, GFaI e. V. and Porsche AG, 2018.

[13] P. SIJTSMA: *CLEAN based on spatial source coherence*. AIAA Paper 2007-3436, 2007.